haematologica
Journal of the Ferrata Storti Foundation

m6a and NuRD complexes regulate monocytic differentiation and resistance to BCL2/BCL2L1 inhibitors in acute myeloid leukemia

by Jackson Brim-Edwards, Karen Morris, Quinlan Morrow, Stephen E. Kurtz, Daniel Bottomly, Shannon K. McWeeney, Cristina E. Tognon, Tamilla Nechiporuk, Kevin Watanabe-Smith and Jeffrey W. Tyner

Received: April 9, 2025.
Accepted: October 3, 2025.

Citation: Jackson Brim-Edwards, Karen Morris, Quinlan Morrow, Stephen E. Kurtz, Daniel Bottomly, Shannon K. McWeeney, Cristina E. Tognon, Tamilla Nechiporuk, Kevin Watanabe-Smith and Jeffrey W. Tyner. m6a and NuRD complexes regulate monocytic differentiation and resistance to BCL2/BCL2L1 inhibitors in acute myeloid leukemia.
Haematologica. 2025 Oct 16. doi: 10.3324/haematol.2025.287972 [Epub ahead of print]

m6a and NuRD complexes regulate monocytic differentiation and resistance to BCL2/BCL2L1 inhibitors in acute myeloid leukemia

Jackson Brim-Edwards[1,2], Karen Morris[1,2], Quinlan Morrow[1,2], Stephen E. Kurtz[2,3], Daniel Bottomly[2], Shannon K. McWeeney[2,3,4], Cristina E. Tognon[2,3], Tamilla Nechiporuk[1,2], Kevin Watanabe-Smith[# 2,3], Jeffrey W. Tyner[# 1,2,5]

[1] Department of Cell, Developmental & Cancer Biology, Oregon Health & Science University, Portland, OR, USA

[2] Knight Cancer Institute, Oregon Health & Science University, Portland, OR, USA

[3] Division of Oncological Sciences, Knight Cancer Institute, Oregon Health & Science University, Portland, OR, USA

[4] Division of Bioinformatics and Computational Biology, Department of Medical Informatics and Clinical Epidemiology, Oregon Health & Science University, Portland, OR, USA

[5] Division of Hematology and Medical Oncology, Oregon Health & Science University, Portland, OR, USA

# These authors contributed equally to this work

Running title: *m6A and NuRD regulate monocytic resistance in AML*

Corresponding author: Jeffrey W. Tyner - Email: tyner@ohsu.edu

Authors' Contributions

J. Brim-Edwards: Investigation, software, validation, data analysis, visualization, writing – original draft **K. Morris:** Investigation, validation **Q Morrow:** Investigation, validation **S. Kurtz:** CRISPR data analysis and methodology, investigation **D. Bottomly:** CRISPR screen data processing workflow methodology and Tiering pipeline **S.K. McWeeney:** CRISPR screen data processing workflow methodology and Tiering

pipeline **T. Nechiporuk:** Conceptualization, CRISPR screen and methodology, investigation, validation **K. Watanabe-Smith:** Conceptualization, software, visualization, data analysis, writing – review and editing **J.W. Tyner: C.E. Tognon:** Conceptualization, resources, supervision, funding acquisition, writing – review and editing.

Acknowledgments

We thank all patients for their generous participation. We also thank the Massively Parallel Sequencing Shared Resource for Illumina sequencing support and the Flow Cytometry Core at Oregon Health & Science University.

Data Availability

The datasets generated and analyzed during the current study are available as follows: CRISPR screen data have been deposited in the Gene Expression Omnibus (GEO) under accession number GSE294240. All other data supporting the findings of this study are provided in the supplementary information. Code used to generate the figures and analyses is available at https://github.com/jbrimed/m6a-nurd-aml-resistance.

Funding

This work was supported by the Acquired Resistance to Therapy Network (ARTNet), National Institutes of Health (NIH), National Cancer Institute (NCI) grant U54CA224019. This work was additionally supported by NCI award R01CA262758 (JWT, SEK.), the Waldman Family Fund for AML Research (JWT), the George Ettelson Endowed Professorship In Acute Myeloid Leukemia Research (JWT), the Mark Foundation for Cancer Research (JWT), and the Silver Family Foundation (JWT).

Disclosures

JWT received research support from Acerta, Agios, Aptose, Array, AstraZeneca, Constellation, Genentech, Gilead, Incyte, Janssen, Kronos, Meryx, Petra, Schrodinger, Seattle Genetics, Syros, Takeda, and Tolero and serves on the advisory board for Recludix Pharm, AmMax Bio, and Ellipses Pharma.

Abstract

Frontline use of the BCL2 inhibitor, venetoclax, for acute myeloid leukemia (AML) has resulted in broad improvements in patient outcome. A major remaining challenge is the development of venetoclax resistance, frequently driven by compensatory transcriptional programs that promote cell survival and differentiation. These changes reduce dependence on BCL2 in favor of alternative anti-apoptotic BCL2 family members such as MCL1 or BCL2L1 (BCL-X_L). Using CRISPR-based genome-wide perturbation screens, we investigated the genetic dependencies of venetoclax and the BCL2/BCL2L1 dual inhibitor AZD4320. We identified the N6-methyladenosine (m6A) writer RBM15*,* and the Nucleosome Remodeling and Deacetylase (NuRD) complex interactor ZMYND8 as novel mediators of resistance to both venetoclax and AZD4320. Loss of *RBM15* or *ZMYND8* induced drug resistance, concurrent with alterations in BCL2 family expression and monocytic differentiation. Accordingly, in AML patient samples we found reduced expression of the respective m6a or NuRD complexes was significantly associated with monocytic differentiation and *ex vivo* resistance to the same drugs. These findings provide critical insights into previously undescribed mechanisms of BCL2 family inhibitor resistance in AML.

Introduction

The BCL2 family of apoptosis regulators has emerged as a promising therapeutic target in AML.[1] This family includes anti-apoptotic proteins such as BCL2, MCL1, and BCL2L1 (BCL-X_L), which block apoptosis by binding and neutralizing pro-apoptotic effectors BAX and BAK—proteins essential for mitochondrial outer membrane permeabilization.[2] Venetoclax, a BH3 mimetic that selectively binds and inhibits BCL2, has demonstrated significant efficacy in AML and is FDA-approved for use in combination with hypomethylating agents to improve response rates and overall survival.[3–6]

Prior CRISPR-based genome-wide perturbation screens have identified key genes and pathways that mediate the response to venetoclax. Downregulation of pro-apoptotic effectors—BAX, PMAIP1 (NOXA), and TP53—or compensatory upregulation of MCL1 and BCL2L1, results in venetoclax-resistance in AML cells.[5,7,8] Cellular differentiation state has also been implicated in resistance, with more differentiated monocytic or megakaryocytic/erythroid cells displaying increased resistance to venetoclax, often accompanied by upregulation of MCL1, BCL2L1, or BCL2A1 relative to BCL2.[8–18] These findings underscore the importance of addressing both changes in the baseline expression of BCL2 proteins and the upregulation following treatment, such as treatment-induced resistance. To address one avenue of resistance, BCL2L1 (BCL-X_L) overexpression, dual inhibitors targeting both BCL2 and BCL2L1—including AZD4320 and Navitoclax—have been developed.[19,20] To identify both shared and unique mechanisms of resistance between AZD4320 and those previously identified for venetoclax, we performed a genome-wide CRISPR/Cas9 screen in OCI-AML2 cells cultured with AZD4320. Here, we identify RBM15 and ZMYND8 as novel key dependencies for the response to both venetoclax and AZD4320.

RBM15 is a component of the m6A RNA methylation machinery, the most common internal mRNA modification, which regulates transcript splicing, export, stability, translation, and degradation. The core m6A “writer” methyltransferase complex includes METTL3, METTL14, and WTAP, with RBM15 acting as an adaptor to recruit

the complex to specific RNA sites. m6A “reader” proteins, such as YTHDF family members, mediate the effects of m6A on RNA metabolism, while “erasers” like FTO and ALKBH5 reverse the modification, dynamically regulating transcript expression.[21,22] In leukemia, the t(1;22)(p13;q13) translocation results in a *RBM15-MKL1* (OTT-MAL) fusion gene, which is linked to a rare subtype of acute megakaryoblastic leukemia (AMKL) in infants.[23]

ZMYND8, a multifunctional epigenetic regulator within the NuRD complex, modulates chromatin structure and transcriptional repression. The NuRD complex, composed of histone deacetylases (HDAC1/2), chromatin remodeling ATPases (CHD3/4), and metastasis-associated proteins (MTA1-3), facilitates chromatin compaction and gene silencing.[24,25] ZMYND8 mediates NuRD complex targeting to specific histone modifications including H3K36me2/3 and H4K16Ac. Recent studies have identified NuRD[26] and ZMYND8[27,28] as essential for AML cell survival by regulating transcriptional programs crucial for leukemogenesis.

In AML, dysregulation of m6A methylation has been implicated in leukemogenesis by modulating the expression of genes involved in self-renewal and differentiation of hematopoietic stem and progenitor cells (HSPCs).[29,30] Similarly, dysregulated NuRD activity alters the expression of genes critical for myeloid maturation, thereby maintaining leukemic cells in an undifferentiated state.[31]

Methods

Cell Lines and Culture Conditions

OCI-AML2 human AML cell lines were obtained from the American Type Culture Collection (ATCC). Cells were cultured in RPMI-1640 medium supplemented with 20% fetal bovine serum, L-glutamine, penicillin-streptomycin, and amphotericin B. Cultures

were maintained at 37 °C with 5% CO_2 and were routinely tested for mycoplasma contamination.

Genome-Wide CRISPR/Cas9 Screening

Loss-of-function screens were performed using the Y. Kosuke[32] human genome-wide sgRNA library. Cells were treated with 30 nM AZD4320 or DMSO control for 14 days. Genomic DNA was extracted, and sgRNA sequences were amplified for Illumina sequencing. Reads were trimmed using cutadapt (v2.3)[33] to extract the candidate sequences. Alignment was then performed using Bowtie2 (v2.3.5.1)[34] relative to a custom set of expected sgRNA sequences. After conversion to Bam format, unique matches were selected using Bamtools (v2.5.1).[35] Reads were counted for each sample using MAGeCK. The counts were next filtered for low representation (those not in the Plasmid-only samples or those with < =100 counts per million in more than half the samples) and then were normalized using Trimmed Mean of M (TMM). The edgeR package[36] was used for each linear model, generating log2 fold changes (LFC) and 2-sided P-values. Gene-level tiering was performed as described previously.[7]

Generation and Validation of Knockout Cell Lines

RBM15 and ZMYND8 knockout cell lines were generated by transducing OCI-AML2 cells with sgRNA-containing lentiviral particles. Two biologically distinct lines were generated for each condition using separate sgRNA sequences. Puromycin selection was applied for 7 days. Knockout efficiency was validated via Western blotting.

Cell Proliferation Assays

Wild-type, non-targeting control, RBM15 knockout, and ZMYND8 knockout OCI-AML2 cells were cultured for 6 days in 30 nM AZD4320 or DMSO. Viable cells were counted every 2 days to assess proliferation.

RNA Sequencing and Analysis

Total RNA was extracted from wild-type, non-targeting control, RBM15 knockout, and ZMYND8 knockout cells. Stranded poly(A)+ RNA sequencing libraries were prepared and sequenced in triplicate on an Illumina NovaSeq 6000 platform, generating 150 bp paired end reads. Reads were trimmed using Trimmomatic and aligned to the human reference genome (GRCh38/hg38) using STAR aligner. Differential expression analysis was performed using DESeq2, with surrogate variable analysis applied for batch effect correction. Genes with an adjusted p-value < 0.05 and an absolute $\log_2$ fold change > 1 were considered differentially expressed. Cell type enrichment was analyzed using the Panglao DB database in R.

BCL2 family gene ratios were calculated as a ratio of normalized counts using DESeq2's median of ratios normalization. Statistical significance was calculated as a two-sided Student's t-Test comparing the six values from the NT lines (two biological lines, three replicates each) to the six values of the indicated knockout line.

Human Subject Data and Ethical Approval

Patient data used in this study was obtained from the publicly available Beat AML dataset, which includes de-identified clinical data. Use of this dataset was approved by the Oregon Health

& Science University Institutional Review Board (IRB). All protocols involving human subject data were conducted in accordance with the ethical standards of the OHSU IRB.

Results

Genome-wide CRISPR screen reveals novel transcriptional regulators controlling BCL2 inhibitor resistance

While acquired resistance to venetoclax supports the development of dual BCL2/BCL2L1 inhibitors(Figure 1A), it is unknown whether unique predictors of drug response exist for BCL2-selective inhibitors versus BCL2/BCL2L1 inhibitors. To address this question, we first analyzed data from *ex vivo* screening of primary AML samples. This approach demonstrated a robust relationship between responses to venetoclax

and AZD4320 for individual patient samples (Figure 1B). By integrating *ex vivo* AZD4320 screening of 232 primary AML samples with the existing Beat AML transcriptomic dataset, we directly compared the correlations between gene expression and drug response in a shared set of samples. While slight outliers were observed, the correlations between gene expression and AUC for venetoclax were largely similar in both direction and magnitude to those observed for AZD4320 (Figure 1C).

To investigate global resistance mechanisms for AZD4320, we conducted a genome-wide CRISPR screen in OCI-AML2 cells treated with 30 nM AZD4320 for 14 days (Figure 2A). We identified several shared, evidence based tiered hits between both AZD4320 and venetoclax[7] screens, including drug-resistance following loss of *PMAIP1*, *BAX* and *TP53*, and increased sensitivity following loss of *BCL2L1* (Figure 2B). Relatively few genes produced discordant hits between the screens, and while promising for future study, the smaller effect sizes in this group led us to prioritize investigation of the strongest shared hits.

Notably, we identify two novel Tier 1 hits, *RBM15* and *ZMYND8*, as regulators of drug response in both the AZD4320 and venetoclax screens.[7,15] To validate these findings, we generated *RBM15* and *ZMYND8* KO OCI-AML2 cell lines using lentiviral CRISPR-Cas9 gene editing, with successful knockout confirmed via Western blotting (Figure S1A). These cells displayed significantly increased resistance (one-way ANOVA with Dunnett's test: RBM15 $p = 0.0001$, ZMYND8 $p = 0.0075$) to AZD4320 compared to NT cells in outgrowth assays (Figure 2C, Figure S1B) and dose-response analyses (Figure S1C-D) compared to non-targeting (NT) controls. Notably, response to non-BCL2 directed inhibitors (including trametinib, midostaurin, and sorafenib) were not similarly affected by loss of *RBM15* or *ZMYND8* (Figure S1E).

RBM15 and ZMYND8 knockout drives changes in BCL2 expression and differentiation consistent with primary AML samples

To examine the mechanisms by which loss of RBM15 or ZMYND8 confers resistance to BCL2 inhibitors, we first performed RNA-sequencing on OCI-AML2 knockout cell lines, followed by Gene Set Enrichment Analysis (GSEA) to identify pathways previously implicated in venetoclax resistance (Figure S2A-B). There appeared to be little upregulation of the pathways commonly associated with drug resistance to BCL2 inhibitors such as *MAPK/ERK* and *TP53* pathways.

The relative ratios of BCL2 family member expression are highly predictive of *in vitro* and clinical venetoclax response, where cells with lower ratios of *BCL2* relative to *BCL2L1* or *MCL1* are resistant to venetoclax.[37–39] Accordingly, we next examined relative RNA expression of BCL2 family members following the knockout of *RBM15* or *ZMYND8*. In *ZMYND8* KO cell lines we indeed detected a reduction in the ratio of *BCL2* to *MCL1* ($p = 0.001$, $t = 4.73$) and *BCL2* to *BCL2A1* ($p < 0.0001$, $t = 9.72$), suggesting an increased reliance on these *BCL2* alternatives for evading drug-induced apoptosis (Figure 3A). Interestingly, in *RBM15* KO cell lines, we did not detect changes in any of the pro-survival members of the BCL2 family, but instead we observed elevated ratios of *BCL2L1* to *BCL2L11* (*BIM*) ($p = 0.002$, $t = -4.51$) and *BCL2* to *BIM* ($p = 0.0006$, $t = -5.06$), suggesting a novel resistance mechanism whereby the increased proportion of pro-survival BCL2 family members relative to the apoptotic initiator BIM may shift the balance toward survival, reducing apoptotic priming and limiting drug efficacy.

We next explored whether these changes in BCL2 family expression in the setting of *RBM15*- and *ZMYND8*-loss are linked to altered AML cell maturation state and assessed whether knockout of these genes influenced differentiation. GSEA of upregulated genes in KO cell lines, using PanglaoDB-derived cell type annotations[40], revealed enrichment of differentiated myeloid cell states in both *RBM15*- and *ZMYND8*-KO lines (Figure 3B). These included macrophage-like (NES = 2.28, FDR = 1.80e-7), monocytic-like (NES = 2.17, FDR = 4.29e-5), and dendritic-like cell types (NES = 2.21, FDR = 1.12e-5).

To further investigate the relationship between *RBM15* and *ZMYND8* expression and differentiation, we evaluated their association with clinical differentiation markers in primary AML samples. Using linear regression, we found that lower expression of both genes was significantly associated with increased percentages of peripheral blood monocytes (*RBM15*: $t = -5.45$, $p < 9.19\times10^{-8}$; *ZMYND8*: $t = -2.92$, $p < 0.003$), consistent with a more differentiated phenotype (Figure 4A). Next, expression of these genes was compared to expression-derived AML-specific cell state scores.[41] Spearman correlation analysis revealed that *RBM15* and *ZMYND8* expression were positively associated with more primitive states, including progenitor-like (*ZMYND8*: $\rho = 0.18$, FDR $< 3.14\times10^{-5}$; *RBM15*: $\rho = 0.16$, FDR $< 1.8\times10^{-4}$) and HSC-like states (*ZMYND8*: $\rho = 0.17$, FDR $< 8.2\times10^{-5}$; *RBM15*: $\rho = 0.23$, FDR $< 1.62\times10^{-5}$). Conversely, both genes were negatively correlated with more differentiated states such as promonocytic-like (*ZMYND8*: $\rho = -0.23$, FDR $< 2.14\times10^{-7}$; *RBM15*: $\rho = -0.11$, FDR $< 1.18\times10^{-2}$) and monocyte-like phenotypes (*ZMYND8*: $\rho = -0.17$, FDR $< 7.77\times10^{-5}$; *RBM15*: $\rho = -0.10$, FDR $< 1.35\times10^{-5}$) (Figure 4A, Figure S3B-C,E-F).

Given that differentiation status is a known predictor of venetoclax sensitivity[8–10,12], we wanted to see if a similar effect was observed with AZD4320. Using Spearman correlation, we observed a positive association between PB monocyte percentages from primary AML samples and AZD4320 response ($\rho = 0.51$, $p < 1.12\times10^{-5}$), consistent with previously reported venetoclax sensitivity patterns (Figure 4B, Figure S3A,D).

In contrast to cell line models, where gene expression and drug response were strongly linked, we found that Spearman correlations between ex vivo venetoclax or AZD4320 response and *RBM15* or *ZMYND8* expression in primary samples were weak or non-significant (venetoclax: *RBM15*: $\rho = -0.009$, FDR = 0.85; *ZMYND8*: $\rho = -0.14$, FDR < 0.004; AZD4320: *RBM15*: $\rho = -0.11$, FDR = 0.094; *ZMYND8*: $\rho = -0.15$, FDR < 0.02) (Figure 4C). Protein abundance of ZMYND8 showed a modest but stronger inverse correlation with drug response, while RBM15 protein expression remained non-significant (Figure S2C–F).

Expanded analysis of m6A RNA methylation and NuRD chromatin remodeling complexes

Given that *RBM15* and *ZMYND8* expression as individual genes did not strongly correlate with drug response in patient samples, we expanded our analysis to include the broader m6A RNA methylation and NuRD chromatin remodeling complexes, where RBM15 and ZMYND8 serve as key components. Using either RNA-seq (Figure S4A) or whole-proteome quantification (LC-MS/MS) of patient samples (Figure 5A,6A), we performed principal component analysis (PCA) to generate eigengene-like signatures for each complex(Table S1), capturing overall pathway activity through unsupervised composite profiles.

Principle Component Analysis of m6A and NuRD Complexes

To assess m□A pathway activity, we performed principal component analysis (PCA) on protein abundance data for core m□A complex members, generating an eigengene-like representation of pathway activity (m□A PC1; Figure 5A). Most proteins loaded positively onto PC1, supporting its interpretation as a proxy of overall m□A complex activity. Linear regression analysis revealed that m□A PC1 was negatively associated with peripheral blood (PB) monocyte percentage (t = -2.25, FDR < 0.03) and positively associated with PB blast percentage[42] (t = 7.89, FDR < 1×10^{-11}), suggesting that reduced m□A pathway activity corresponds to more differentiated cell states (Figure 5B).

Similarly, principal component analysis (PCA) of NuRD complex protein abundance generated a NuRD eigengene-like signature (NuRD PC1), representing overall pathway activity (Figure 6A). Most pathway components loaded positively onto PC1, analogous to the m□A analysis. Using linear regression, we found that NuRD PC1 was negatively associated with peripheral blood (PB) monocyte percentage (t = -3.64, FDR < 7.55×10^{-4}) and positively associated with PB blast percentage (t = 5.54, FDR < 7.1×10^{-7}), supporting the interpretation that reduced NuRD complex activity corresponds to a more differentiated disease state.

Both of these pathway principal components correlated with expression-derived AML cell state scores[41], which reinforced these findings. Spearman correlation analysis demonstrated that the m□A PC1 was strongly negatively correlated with monocyte-like states (ρ = -0.68, FDR < 1.04×10-17) and positively correlated with primitive states, including progenitor-like (ρ = 0.70, FDR < 2.55×10^{-19}) and HSC-like states (ρ = 0.28, FDR < 1.03×10^{-3}; Figure 5B). Similarly, NuRD PC1 was negatively correlated with monocyte-like states (ρ = -0.59, FDR < 5.6×10^{-13}) and positively correlated with progenitor-like (ρ = 0.62, FDR < 1.1×10^{-14}) and HSC-like states (ρ = 0.44, FDR < 3.2×10^{-7}; Figure 6B). These data collectively support a model in which reduced m□A and NuRD complex activities are linked to more differentiated AML cell states, consistent with their proposed roles in maintaining cellular primitiveness.

Drug sensitivity analysis

To explore the potential therapeutic impact of these pathways, we assessed the correlation between each principal component and *ex vivo* response to several small molecule inhibitors in primary AML samples. Both the m6A and NuRD PC1s were negatively correlated with sensitivity to AZD4320 (m6A: ρ = -0.49, FDR < $3.7x10^{-4}$; NuRD: ρ = -0.48, FDR < 6.72 $x10^{-4}$) and venetoclax (m6A: ρ = -0.49, FDR < 5.3 $x10^{-6}$; NuRD: ρ = -0.49, FDR < 6.9 $x10^{-6}$) (Figures 5C, 6C). These findings suggest that reduced m6A and NuRD pathway activity is associated with resistance to BCL2 inhibitors, consistent with prior observations that differentiated AML subtypes are less sensitive to these therapies. This setting of reduced expression of m6A or NuRD pathways does correlate with sensitivity to certain drugs, including inhibitors of HDACs (Panobinostat), MTOR (Rapamycin), and a kinase inhibitor (nilotinib). Similar analyses using RNA data to generate expression derived principal component scores yielded comparable results for both pathways (Figure S4A-F).

Overall, these findings highlight the strong link between m6A and NuRD pathway activities and AML differentiation, demonstrating that reduced pathway activity or

disruption contributes to decreased sensitivity to BCL2 inhibitors in a differentiation-dependent manner.

Discussion

Venetoclax, a selective BCL2 inhibitor, has significantly advanced the treatment of AML, particularly in older patients unfit for intensive chemotherapy, when used in combination with hypomethylating agents. However, despite promising initial responses, resistance to venetoclax remains a major clinical hurdle, leading to relapse in many patients. Here, we identify *RBM15* and *ZMYND8* as novel mediators of resistance to both venetoclax and the dual BCL2/BCL2L1 inhibitor AZD4320 in the OCI-AML2 cell line. Notably, the loss of either gene induces differentiation toward a monocytic phenotype, resulting in resistance to BCL2 inhibition. This observation aligns with previous findings that more differentiated AML cells exhibit inherent resistance to venetoclax.[8–18]

Using genome-wide CRISPR screens, we confirmed that apoptotic regulators known to control the response to venetoclax, such as *BAX*, *PMAIP1*, and *TP53*[7], are similarly involved in the response to AZD4320. While highly similar drugs, primary samples indicate expression of a few genes are more correlated to venetoclax response including *BCL2*, *TP53BP1*, and *IL6ST*. Genes more predictive of AZD4320 response include *MCOLN1* (which inhibits apoptosis in a BAX-dependent manner) and *SEMA4G*.[43] Notably *SEMA4G* is not linked to the BCL2 family, but the intron of *SEMA4G* contains *miR-608*, which promotes apoptosis in prostate cancer cells by inhibiting *BCL2L1* translation through directly binding the 5'UTR.[44] We are unable to detect expression of the short *miR-608* in our poly-A enriched RNAseq dataset, but expression of *SEMA4G* could be acting as a proxy for increased transcription of miR-608. Post-transcriptional control of *BCL2L1* by *miR-608* could also account for the lack of any observed correlation between *BCL2L1* expression and response to venetoclax or AZD4320 in patient samples.

Resistance to AZD4320 in our knockout cell lines appeared to be driven by monocytic differentiation along with alterations in the expression ratios of BCL2 family members, which has previously been shown to be associated with venetoclax resistance.[38] *ZMYND8*-KO lines show a reduction in BCL2 expression, especially relative to *MCL1* or *BCL2A1*, indicating a shift away from venetoclax and AZD4320 drug targets towards untargeted anti-apoptotic BCL2 members. This is consistent with the MAC-score previously shown to be predictive of clinical venetoclax response when assessing relative protein abundance of *BCL2* vs *MCL1* and *BCL2L1*.[38] Conversely, *RBM15*-KO cells show no shift away from *BCL2* or *BCL2L1*; instead, these cells have reduced expression of the pro-apoptotic initiator *BCL2L11* (*BIM*), while increasing expression of the drug targets in a novel manner unique from prior known mechanisms of venetoclax resistance. These divergent expression changes suggest that different resistance mechanisms may necessitate distinct therapeutic strategies. For example, the setting of *ZMYND8* deficiency-related resistance would call for combining BCL2 inhibition with MCL1/BCL2A1 targeting agents. In contrast, for RBM15 deficiency related cases of resistance, effective targeting strategies could include BIM stabilization or alternative apoptotic priming approaches.

Mutations and signaling activation in the *RAS/MAPK* pathway have been previously shown to result in venetoclax resistance *in vitro* and *in vivo.*[45] Notably, we see no indication of activated *RAS/MAPK*-signaling in either knockout cell line by GSEA for signaling signatures (Figure S2A-B), nor do we see altered response to RAF (sorafenib) or MEK (trametinib) inhibitors following knockout (Figure S1F), demonstrating a RAS-independent mode of BCL2 inhibitor resistance. Taken together with the findings above, we conclude monocytic-differentiation with associated changes in BCL2 family expression is the primary mechanism towards resistance to venetoclax and AZD4320 in m6a- and NuRD-disrupted settings.

RBM15 is a member of the m6A RNA methylation complex, which regulates mRNA stability and translation through N6-methyladenosine (m6A) modifications. Previous studies have highlighted the role of m6A modifications in controlling myeloid

differentiation and leukemogenesis. For instance, METTL3-mediated m6A methylation maintains the undifferentiated state of AML cells by promoting the translation of *MYC* and *BCL2* transcripts.[21] Loss of *RBM15* may disrupt m6A methylation patterns, leading to altered expression of genes that promote differentiation, thereby reducing susceptibility to apoptosis induced by BCL2 inhibitors.

Similarly, ZMYND8 is part of the NuRD chromatin remodeling complex, which influences transcriptional repression and chromatin accessibility. The NuRD complex modulates gene expression programs essential for myeloid maturation.[31] Loss of *ZMYND8* could result in depression of differentiation-associated genes, promoting a monocytic phenotype less susceptible to BCL2 inhibition. Interestingly, ZMYND8 has been identified as a potential therapeutic target in AML. Previous work has shown that ZMYND8 regulates the IRF8 transcription axis and is an AML dependency, suggesting that its inhibition could impair leukemia cell proliferation.[46] However, our findings introduce a critical consideration: while targeting ZMYND8 may reduce proliferation, it may also induce differentiation-associated resistance to current frontline BCL2 inhibitors like venetoclax and AZD4320.

Our analyses of patient-derived AML samples revealed that lower expression levels of *RBM15* and *ZMYND8* correlated with more differentiated, monocyte-like cell states. We did not find a significant direct association between their expression levels and sensitivity to venetoclax or AZD4320, in contrast to the strong associations observed in our cell line models. This lack of correlation could be due to idiosyncratic reliance on these specific genes in the cell line models versus broader utilization of the m6a and NuRD family genes in primary patient samples. To address this, we expanded our analysis to include the broader m6A RNA methylation and NuRD chromatin remodeling complexes. Using principal component analysis, we discovered that the activity of these complexes is strongly negatively correlated with drug response to AZD4320 and venetoclax. The m6A and NuRD principal components negatively correlated with monocyte-like states and positively with progenitor-like states, indicating that reduced activity of these pathways is linked to increased differentiation and

consistent with our observed monocytic-shift following *RBM15* or *ZMYND8* knockout. Remarkably, these principal components mapped well onto cell state scores[41], even though these signatures were unsupervised and not designed to match cell state. This underscores the significant influence of m6A RNA methylation and NuRD chromatin remodeling on AML cell differentiation and suggests that these pathways contribute to drug resistance through modulation of cellular differentiation.

Our findings reinforce that the m6A and NuRD complexes are key regulators linking epigenetic and post-transcriptional modifications to AML cell differentiation and drug resistance. Targeting the m6A methylation and NuRD chromatin remodeling pathways could offer new avenues to modulate differentiation and overcome resistance to BCL2 inhibitors, potentially informing treatment plans for clinicians. Exploring combination therapies that modulate differentiation pathways or target differentiated cells while also targeting BCL2 family proteins may enhance treatment efficacy and help circumvent resistance in AML patients.

References

1. Pan R, Hogdal LJ, Benito JM, et al. Selective BCL-2 Inhibition by ABT-199 Causes On Target Cell Death in Acute Myeloid Leukemia. Cancer Discov. 2014;4(3):362-375.

2. Youle RJ, Strasser A. The BCL-2 protein family: opposing activities that mediate cell death. Nat Rev Mol Cell Biol. 2008;9(1):47-59.

3. Pollyea DA, Stevens BM, Jones CL, et al. Venetoclax with azacitidine disrupts energy metabolism and targets leukemia stem cells in patients with acute myeloid leukemia. Nat Med. 2018;24(12):1859-1866.

4. DiNardo CD, Jonas BA, Pullarkat V, et al. Azacitidine and Venetoclax in Previously Untreated Acute Myeloid Leukemia. N Engl J Med. 2020;383(7):617-629.

5. Carter BZ, Mak PY, Mu H, et al. Combined Targeting of BCL-2 and BCR-ABL Tyrosine Kinase Eradicates Chronic Myeloid Leukemia Stem Cells. Sci Transl Med. 2016;8(355):355ra117.

6. Chen X, Glytsou C, Zhou H, et al. Targeting mitochondrial structure sensitizes acute myeloid leukemia to Venetoclax treatment. Cancer Discov. 2019;9(7):890-909.

7. Nechiporuk T, Kurtz SE, Nikolova O, et al. The TP53 Apoptotic Network Is a Primary Mediator of Resistance to BCL2 Inhibition in AML Cells. Cancer Discov. 2019;9(7):910-925.

8. Kuusanmäki H, Dufva O, Vähä-Koskela M, et al. Erythroid/megakaryocytic differentiation confers BCL-XL dependency and venetoclax resistance in acute myeloid leukemia. Blood. 2023;141(13):1610-1625.

9. Pei S, Pollyea DA, Gustafson A, et al. Monocytic Subclones Confer Resistance to Venetoclax-Based Therapy in Patients with Acute Myeloid Leukemia. Cancer Discov. 2020;10(4):536-551.

10. Kuusanmäki H, Leppä A-M, Pölönen P, et al. Phenotype-based drug screening reveals association between venetoclax response and differentiation stage in acute myeloid leukemia. Haematologica. 2020;105(3):708-720.

11. Zeng AGX, Bansal S, Jin L, et al. A cellular hierarchy framework for understanding heterogeneity and predicting drug response in acute myeloid leukemia. Nat Med. 2022;28(6):1212-1223.

12. White BS, Khan SA, Mason MJ, et al. Bayesian multi-source regression and monocyte-associated gene expression predict BCL-2 inhibitor resistance in acute myeloid leukemia. NPJ Precis Oncol. 2021;5(1):71.

13. Zhang H, Nakauchi Y, Köhnke T, et al. Integrated analysis of patient samples identifies biomarkers for venetoclax efficacy and combination strategies in acute myeloid leukemia. Nat Cancer. 2020;1(8):826-839.

14. Pei S, Shelton IT, Gillen AE, et al. A Novel Type of Monocytic Leukemia Stem Cell Revealed by the Clinical Use of Venetoclax-Based Therapy. Cancer Discov. 2023;13(9):2032-2049.

15. Eide CA, Kurtz SE, Kaempf A, et al. Clinical Correlates of Venetoclax-Based Combination Sensitivities to Augment Acute Myeloid Leukemia Therapy. Blood Cancer Discov. 2023;4(6):452-467.

16. Bottomly D, Long N, Schultz AR, et al. Integrative analysis of drug response and clinical outcome in acute myeloid leukemia. Cancer Cell. 2022;40(8):850-864.e9.

17. Kurtz SE, Eide CA, Kaempf A, et al. Associating drug sensitivity with differentiation status identifies effective combinations for acute myeloid leukemia. Blood Adv. 2022;6(10):3062-3067.

18. Majumder MM, Leppä A-M, Hellesøy M, et al. Multi-parametric single cell evaluation defines distinct drug responses in healthy hematologic cells that are retained in corresponding malignant cell types. Haematologica. 2020;105(6):1527-1538.

19. Balachander SB, Criscione SW, Byth KF, et al. AZD4320, A Dual Inhibitor of Bcl-2 and Bcl-xL, Induces Tumor Regression in Hematologic Cancer Models without Dose-limiting Thrombocytopenia. Clin Cancer Res. 2020;26(24):6535-6549.

20. Wilson WH, O'Connor OA, Czuczman MS, et al. Navitoclax, a targeted high-affinity inhibitor of BCL-2, in lymphoid malignancies: a phase 1 dose-escalation study of safety, pharmacokinetics, pharmacodynamics, and antitumour activity. Lancet Oncol. 2010;11(12):1149-1159.

21. Vu LP, Pickering BF, Cheng Y, et al. The N6-methyladenosine (m6A)-forming enzyme METTL3 controls myeloid differentiation of normal hematopoietic and leukemia cells. Nat Med. 2017;23(11):1369-1376.

22. Patil DP, Chen C-K, Pickering BF, et al. m6A RNA methylation promotes XIST-mediated transcriptional repression. Nature. 2016;537(7620):369-373.

23. Ma Z, Morris SW, Valentine V, et al. Fusion of two novel genes, RBM15 and MKL1, in the t(1;22)(p13;q13) of acute megakaryoblastic leukemia. Nat Genet. 2001;28(3):220-221.

24. Xue Y, Wong J, Moreno GT, Young MK, Côté J, Wang W. NURD, a novel complex with both ATP-dependent chromatin-remodeling and histone deacetylase activities. Mol Cell. 1998;2(6):851-861.

25. Li N, Li Y, Lv J, et al. ZMYND8 Reads the Dual Histone Mark H3K4me1-H3K14ac to Antagonize the Expression of Metastasis-Linked Genes. Mol Cell. 2016;63(3):470-484.

26. Najm FJ, DeWeirdt P, Moore MM, et al. Chromatin complex dependencies reveal targeting opportunities in leukemia. Nat Commun. 2023;14(1):448.

27. Yoshida T, Hazan I, Zhang J, et al. The role of the chromatin remodeler Mi-2β in hematopoietic stem cell self-renewal and multilineage differentiation. Genes Dev. 2008;22(9):1174-1189.

28. DepMap B. DepMap 24Q4 Public. https://doi.org/10.25452/figshare.plus.27993248.v1 [Epub ahead of print].

29. Weng H, Huang H, Wu H, et al. METTL14 Inhibits Hematopoietic Stem/Progenitor Differentiation and Promotes Leukemogenesis via mRNA m6A Modification. Cell Stem Cell. 2018;22(2):191-205.e9.

30. Ma X, Renda MJ, Wang L, et al. Rbm15 modulates Notch-induced transcriptional activation and affects myeloid differentiation. Mol Cell Biol. 2007;27(8):3056-3064.

31. Miccio A, Wang Y, Hong W, et al. NuRD mediates activating and repressive functions of GATA-1 and FOG-1 during blood development. EMBO J. 2010;29(2):442-456.

32. Tzelepis K, Koike-Yusa H, De Braekeleer E, et al. A CRISPR Dropout Screen Identifies Genetic Vulnerabilities and Therapeutic Targets in Acute Myeloid Leukemia. Cell Rep. 2016;17(4):1193-1205.

33. Martin M. Cutadapt removes adapter sequences from high-throughput sequencing reads. EMBnet.journal. 2011;17(1):10-12.

34. Langmead B, Salzberg SL. Fast gapped-read alignment with Bowtie 2. Nat Methods. 2012;9(4):357-359.

35. Barnett DW, Garrison EK, Quinlan AR, Strömberg MP, Marth GT. BamTools: a C++ API and toolkit for analyzing and managing BAM files. Bioinformatics. 2011;27(12):1691-1692.

36. Robinson MD, Oshlack A. A scaling normalization method for differential expression analysis of RNA-seq data. Genome Biol. 2010;11(3):R25.

37. Punnoose EA, Leverson JD, Peale F, et al. Expression Profile of BCL-2, BCL-XL, and MCL-1 Predicts Pharmacological Response to the BCL-2 Selective Antagonist Venetoclax in Multiple Myeloma Models. Mol Cancer Ther. 2016;15(5):1132-1144.

38. Waclawiczek A, Leppä A-M, Renders S, et al. Combinatorial BCL2 Family Expression in Acute Myeloid Leukemia Stem Cells Predicts Clinical Response to Azacitidine/Venetoclax. Cancer Discov. 2023;13(6):1408-1427.

39. Touzeau C, Dousset C, Le Gouill S, et al. The Bcl-2 specific BH3 mimetic ABT-199: a promising targeted therapy for t(11;14) multiple myeloma. Leukemia. 2014;28(1):210-212.

40. Franzén O, Gan L-M, Björkegren JLM. PanglaoDB: a web server for exploration of mouse and human single-cell RNA sequencing data. Database (Oxford). 2019;2019:baz046.

41. van Galen P, Hovestadt V, Wadsworth Ii MH, et al. Single-Cell RNA-Seq Reveals AML Hierarchies Relevant to Disease Progression and Immunity. Cell. 2019;176(6):1265-1281.e24.

42. Tyner JW, Tognon CE, Bottomly D, et al. Functional genomic landscape of acute myeloid leukaemia. Nature. 2018;562(7728):526-531.

43. Colletti GA, Miedel MT, Quinn J, Andharia N, Weisz OA, Kiselyov K. Loss of Lysosomal Ion Channel Transient Receptor Potential Channel Mucolipin-1 (TRPML1) Leads to Cathepsin B-dependent Apoptosis. J Biol Chem. 2012;287(11):8082-8091.

44. Zhang X, Fang J, Chen S, Wang W, Meng S, Liu B. Nonconserved miR-608 suppresses prostate cancer progression through RAC2/PAK4/LIMK1 and BCL2L1/caspase-3 pathways by targeting the 3′-UTRs of RAC2/BCL2L1 and the coding region of PAK4. Cancer Med. 2019;8(12):5716-5734.

45. Zhang Q, Riley-Gillis B, Han L, et al. Activation of RAS/MAPK pathway confers MCL-1 mediated acquired resistance to BCL-2 inhibitor venetoclax in acute myeloid leukemia. Signal Transduct Target Ther. 2022;7(1):51.

46. Cao Z, Budinich KA, Huang H, et al. ZMYND8-regulated IRF8 transcription axis is an acute myeloid leukemia dependency. Mol Cell. 2021;81(17):3604-3622.e10.

Figures

Figure 1: AZD4320 overcomes BCL2L1-mediated resistance and mirrors venetoclax sensitivity in AML.
(A) Schematic of the differential action of venetoclax and AZD4320. Upregulation of BCL2L1 (BCL-XL) confers resistance to venetoclax but not to AZD4320. (B) Comparison of AUC values between venetoclax and AZD4320 for 232 AML patient samples from the BEAT AML database. (C) Pearson's correlation of gene expression and ex vivo drug response to venetoclax or AZD4320 for 232 AML patient samples. Signed, log-transformed false discovery rate (FDR) corrected p-values shown for venetoclax (x-axis) and AZD4320 (y-axis). Dotted line indicates x = y line; select BCL2-family genes and outliers labeled.

Figure 2: Genome-wide CRISPR screens identify RBM15 and ZMYND8 as AZD4320 resistance hits. (A) CRISPR screen results display log-fold changes and significance in sgRNA abundance change in OCI-AML2 cells over 14 days of AZD4320 (30 nM) treatment when compared to DMSO-treated controls. Genes are stratified into confidence tiers based on effect size and concordance between multiple guides. (B) Comparison of AZD4320 and venetoclax CRISPR screens on OCI-AML2 cells; genes that were classified as tier 1, 2, or 3 hits in both screens are labeled, including discordant genes (in maroon). (C) Viability of OCI-AML2 cells with single-gene knockouts (KO) while cultured in 30 nM AZD4320; RBM15- and ZMYND8-KO are highlighted in blue and yellow respectively.

Figure 3: RBM15 and ZMYND8 knockout alters apoptotic balance and promotes myeloid differentiation. (A) Ratios of BCL2 family member expression in OCI-AML2 cells following single-gene knockout. Biological replicates generated with distinct sgRNAs are shown for each knockout, and three technical replicates for each line. ZMYND8 KO cells show significant reduction in BCL2 relative to other anti-apoptotic members MCL1 and BCL2A1 (two-sided t-test p-value shown). RBM15 KO cells are significantly increased in expression of AZD4320 targets BCL2L1 and BCL2 relative to the apoptotic initiator BCL2L11 (BIM). (B) Gene Set Enrichment Analysis (GSEA) of differentially expressed genes between RBM15-KO and ZMYND8-KO lines against NT-control lines shows increased enrichment of differentiated myeloid cell states—including neutrophil-like, macrophage-like, and monocyte-like—in both KO lines, with odds ratios (OR) and FDR-adjusted p-values indicating significance.

Figure 4: RBM15 and ZMYND8 expression correlate with progenitor states and BCL2 inhibitor response in BEAT AML patient data. (A) Correlation of RBM15 and ZMYND8 expression with RNA-derived cell differentiation states and clinical data in AML patient samples. Spearman correlation was used for associations with inferred differentiation states, while linear regression was used for clinical variables. Both genes

show higher expression in progenitor-like states and lower expression in more differentiated cell types. The t-statistic reported is derived from our linear regression. Additionally, strong negative correlations were observed between gene expression and monocyte abundance in peripheral blood. (* : p<.05,** : p<.01,*** : p<.001). (B) Association of monocyte abundance in patient samples with drug response (AUC) to venetoclax, AZD4320, and other inhibitors. Both AZD4320- and venetoclax-response are highly correlated with monocyte abundance. (C) Scatter plots of RBM15 and ZMYND8 expression versus ex vivo drug response (AUC) for venetoclax and AZD4320 in primary AML samples, showing no significant Spearman correlation for RBM15 expression and a moderate correlation for ZMYND8 expression with drug sensitivity.

Figure 5: m6A pathway activity from BEAT AML dataset is associated with AML differentiation and drug resistance.
(A) Biplot showing member contribution in the principal component analysis (PCA) of m6A pathway genes' protein levels from the BEAT AML dataset to generate an m6A eigengene-like signature (* : p<.05,** : p<.01,*** : p<.001). (B) Correlation of the m6A PC1 with cell state scores and linear regression against clinical differentiation markers, showing negative associations with more differentiated states. (C) Drug response correlations for the m6A PC1, indicating resistance to AZD4320 and venetoclax (* : FDR<.05,** : FDR<.01,*** : FDR<.001).

Figure 6: Expression of NuRD complex genes reveals a progenitor-linked resistance signature in AML, similar to that seen with m6A pathway activity.
(A) Biplot for PCA of NuRD complex genes to create a NuRD PC1, with individual gene contributions to PC1 and PC2 shown (* : p<.05,** : p<.01,*** : p<.001). (B) Correlation of the NuRD PC1 with cell states and differentiation markers, also highlighting associations with more differentiated cells. (C) Drug response correlations for the NuRD PC1, showing similar resistance patterns to AZD4320 and venetoclax (* : FDR<.05,** : FDR<.01,*** : FDR<.001).

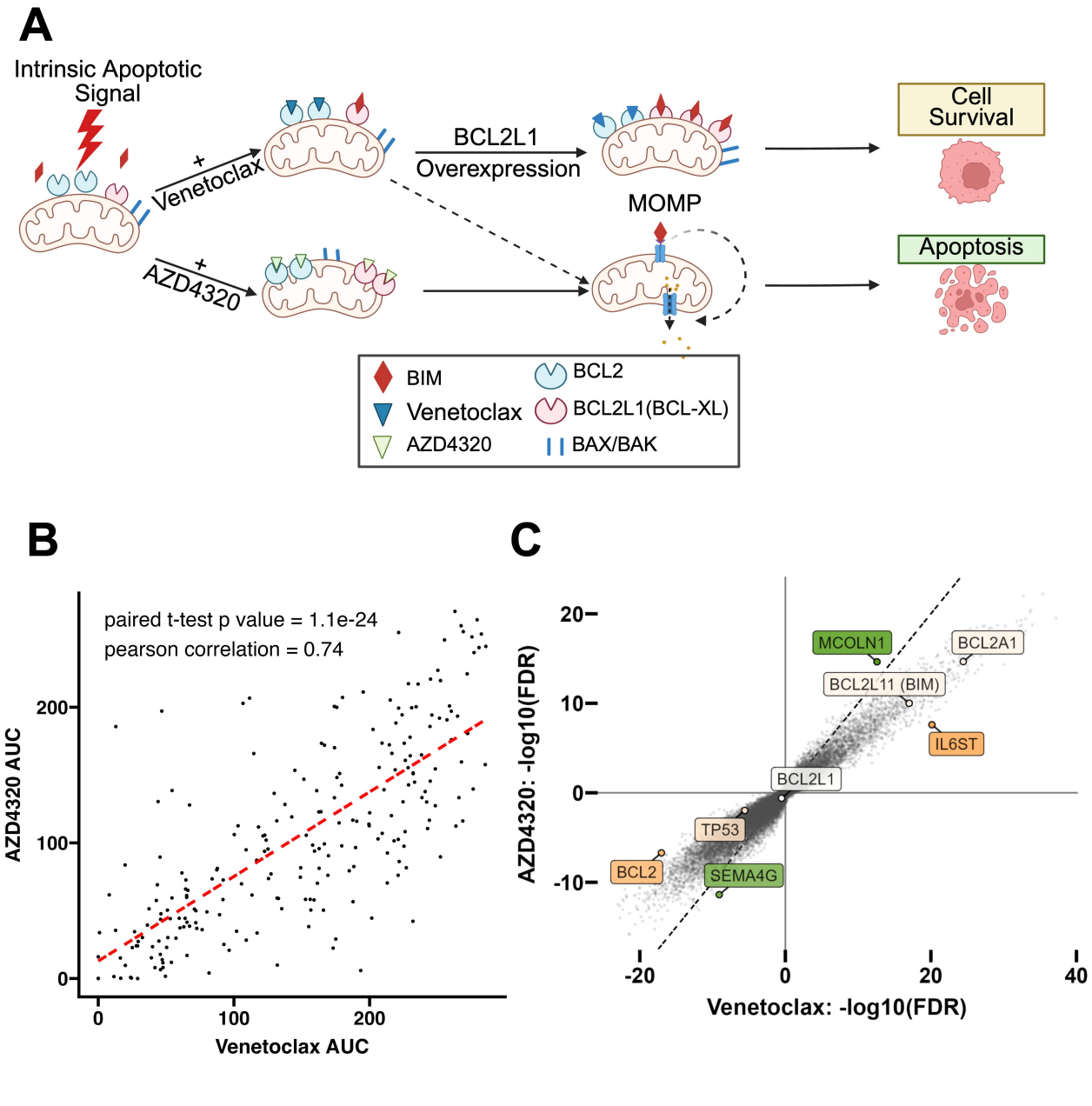
A
Intrinsic Apoptotic Signal
+ Venetoclax
+ AZD4320
BCL2L1 Overexpression
MOMP
Cell Survival
Apoptosis
BIM
Venetoclax
AZD4320
BCL2
BCL2L1(BCL-XL)
BAX/BAK
B
paired t-test p value = 1.1e-24
pearson correlation = 0.74
AZD4320 AUC
Venetoclax AUC
0
100
200
C
AZD4320: -log10(FDR)
Venetoclax: -log10(FDR)
20
10
0
-10
-20
40
MCOLN1
BCL2A1
BCL2L11 (BIM)
IL6ST
BCL2L1
TP53
BCL2
SEMA4G

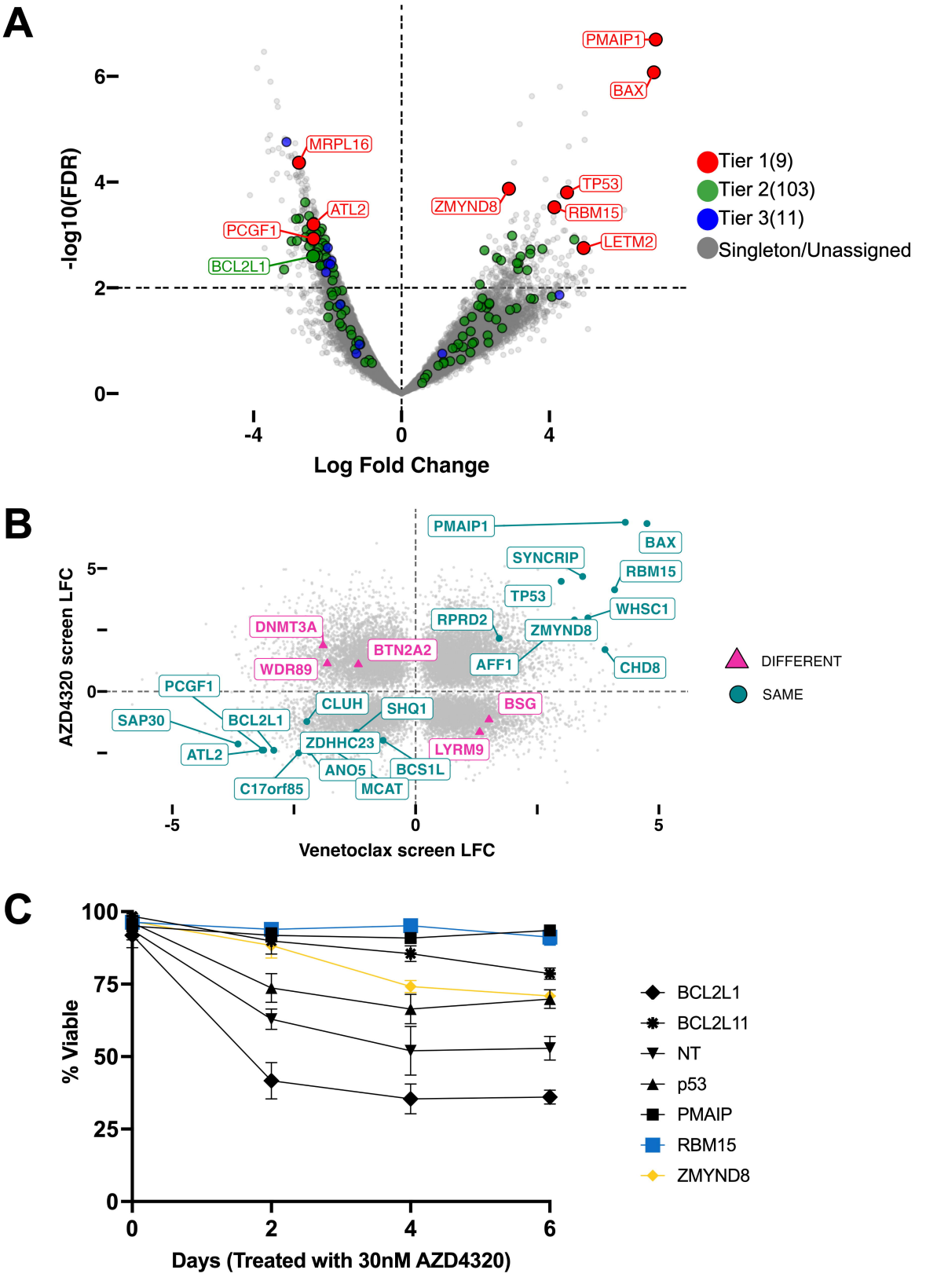
A
PMAIP1
BAX
MRPL16
ATL2
PCGF1
BCL2L1
ZMYND8
TP53
RBM15
LETM2
Tier 1(9)
Tier 2(103)
Tier 3(11)
Singleton/Unassigned
-log10(FDR)
Log Fold Change
B
PMAIP1
BAX
SYNCRIP
RBM15
TP53
WHSC1
RPRD2
ZMYND8
DNMT3A
BTN2A2
AFF1
CHD8
WDR89
PCGF1
CLUH
SHQ1
BSG
SAP30
BCL2L1
ZDHHC23
LYRM9
ATL2
ANO5
BCS1L
C17orf85
MCAT
DIFFERENT
SAME
AZD4320 screen LFC
Venetoclax screen LFC
C
% Viable
Days (Treated with 30nM AZD4320)
BCL2L1
BCL2L11
NT
p53
PMAIP
RBM15
ZMYND8

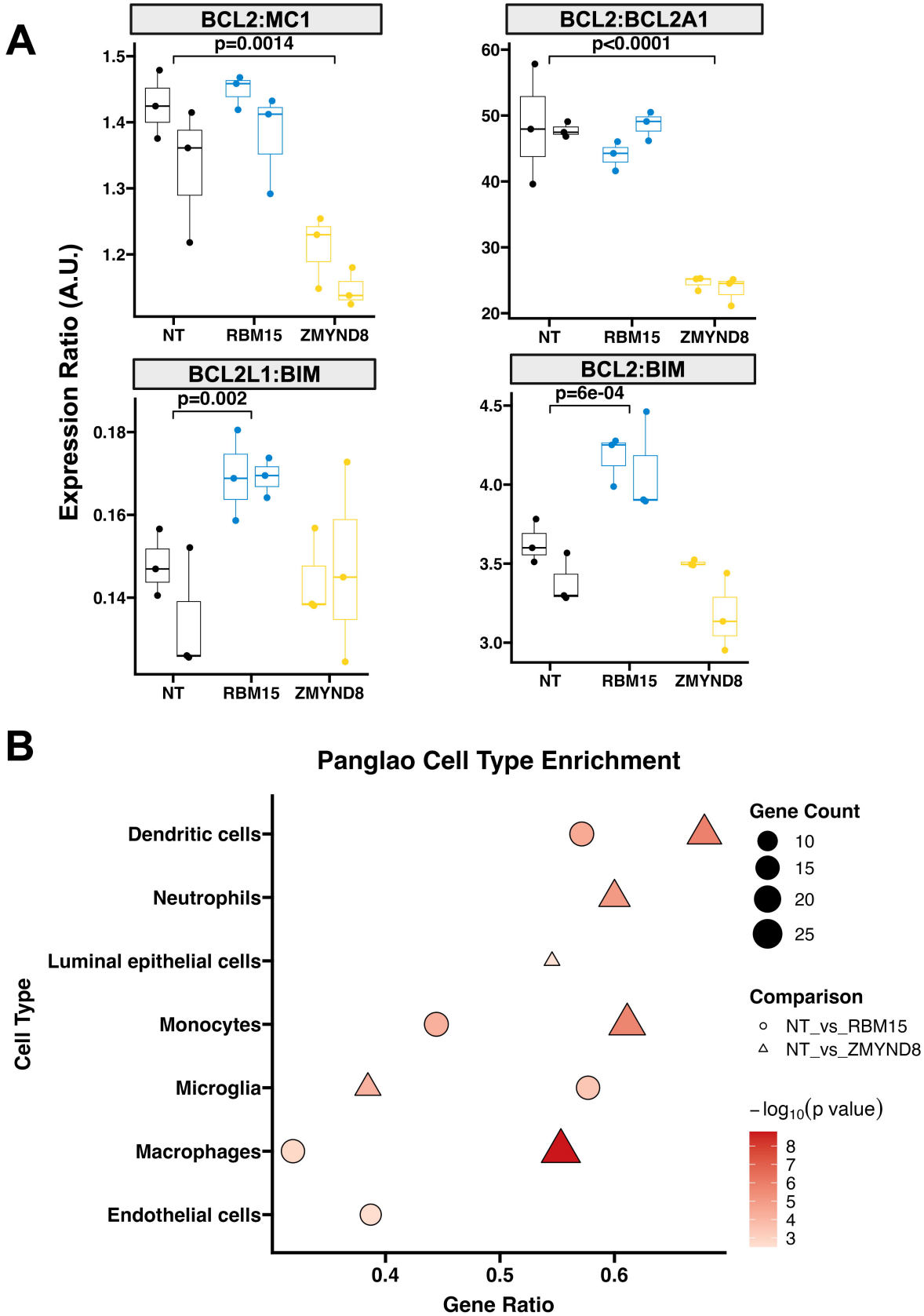
A
BCL2:MC1
p=0.0014
BCL2:BCL2A1
p<0.0001
BCL2L1:BIM
p=0.002
BCL2:BIM
p=6e-04
Expression Ratio (A.U.)
NT
RBM15
ZMYND8
B
Panglao Cell Type Enrichment
Dendritic cells
Neutrophils
Luminal epithelial cells
Monocytes
Microglia
Macrophages
Endothelial cells
Cell Type
Gene Ratio
Gene Count
Comparison
NT_vs_RBM15
NT_vs_ZMYND8
−log10(p value)

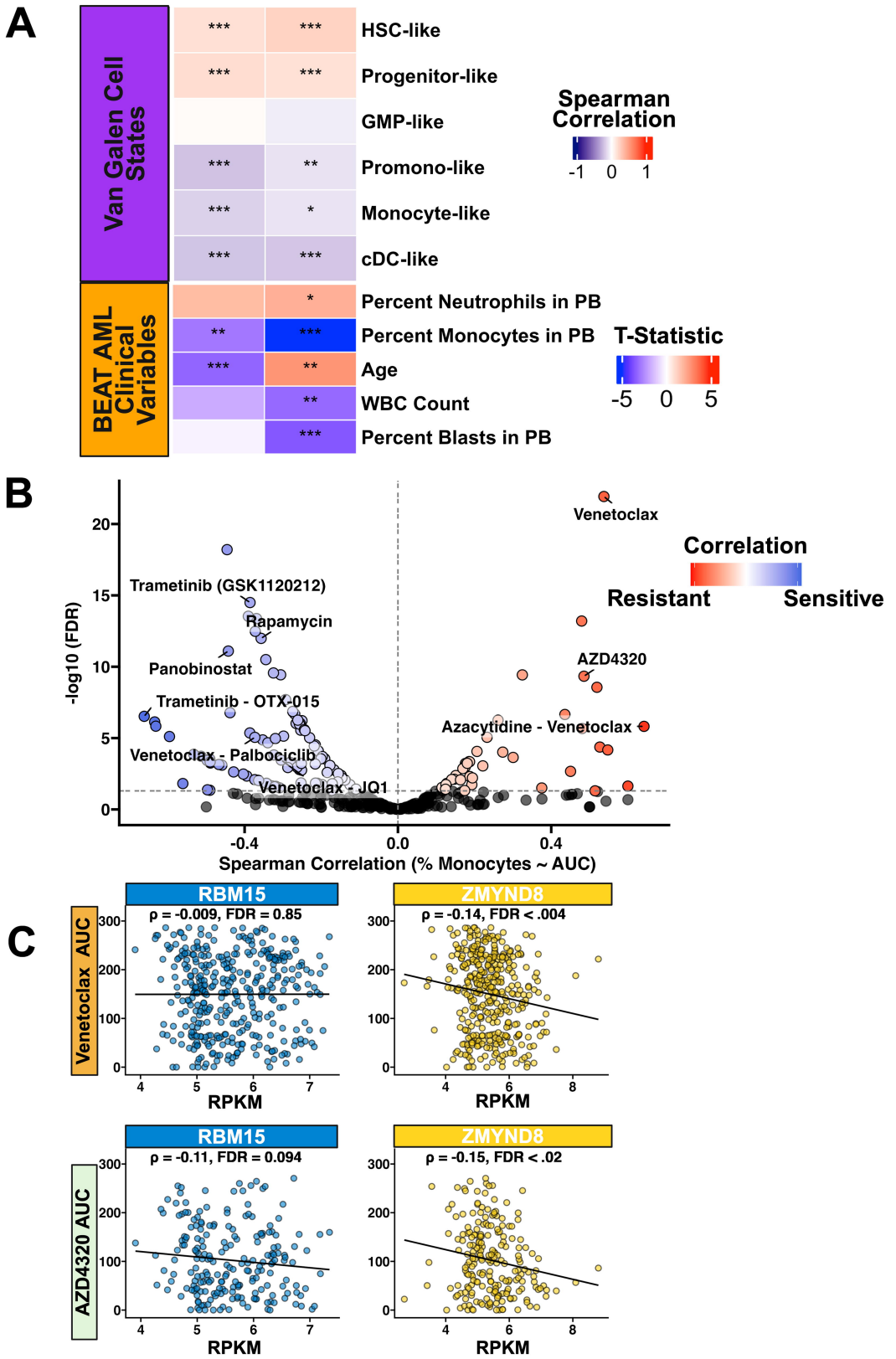
A
Van Galen Cell States
BEAT AML Clinical Variables
HSC-like
Progenitor-like
GMP-like
Promono-like
Monocyte-like
cDC-like
Percent Neutrophils in PB
Percent Monocytes in PB
Age
WBC Count
Percent Blasts in PB
Spearman Correlation
-1 0 1
T-Statistic
-5 0 5
B
Venetoclax
Correlation
Resistant
Sensitive
Trametinib (GSK1120212)
Rapamycin
Panobinostat
Trametinib - OTX-015
Venetoclax - Palbociclib
Venetoclax - JQ1
AZD4320
Azacytidine - Venetoclax
-log10 (FDR)
Spearman Correlation (% Monocytes ~ AUC)
C
RBM15
ρ = -0.009, FDR = 0.85
ZMYND8
ρ = -0.14, FDR < .004
Venetoclax AUC
RBM15
ρ = -0.11, FDR = 0.094
ZMYND8
ρ = -0.15, FDR < .02
AZD4320 AUC
RPKM

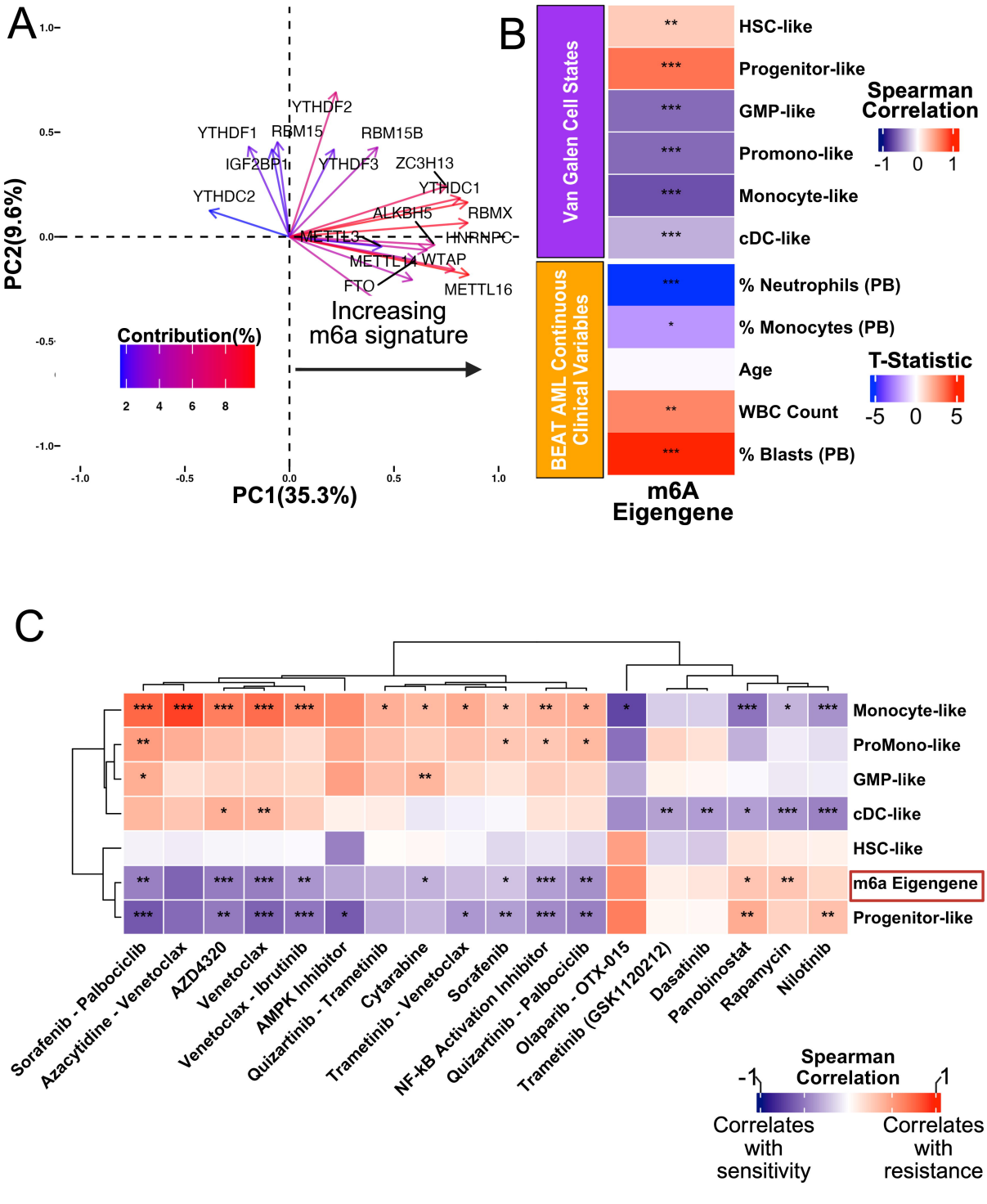
A
PC2(9.6%)
PC1(35.3%)
YTHDF2
YTHDF1
RBM15
RBM15B
IGF2BP1
YTHDF3
ZC3H13
YTHDC1
YTHDC2
ALKBH5
RBMX
METTL3
HNRNPC
METTL14
WTAP
FTO
METTL16
Increasing
m6a signature
Contribution(%)
2 4 6 8
B
Van Galen Cell States
HSC-like
Progenitor-like
GMP-like
Promono-like
Monocyte-like
cDC-like
Spearman
Correlation
-1 0 1
BEAT AML Continuous
Clinical Variables
% Neutrophils (PB)
% Monocytes (PB)
Age
WBC Count
% Blasts (PB)
T-Statistic
-5 0 5
m6A
Eigengene
C
Monocyte-like
ProMono-like
GMP-like
cDC-like
HSC-like
m6a Eigengene
Progenitor-like
Sorafenib - Palbociclib
Azacytidine - Venetoclax
AZD4320
Venetoclax
Venetoclax - Ibrutinib
AMPK Inhibitor
Quizartinib - Trametinib
Cytarabine
Trametinib - Venetoclax
Sorafenib
NF-kB Activation Inhibitor
Quizartinib - Palbociclib
Olaparib - OTX-015
Trametinib (GSK1120212)
Dasatinib
Panobinostat
Rapamycin
Nilotinib
Spearman
Correlation
-1
1
Correlates
with
sensitivity
Correlates
with
resistance

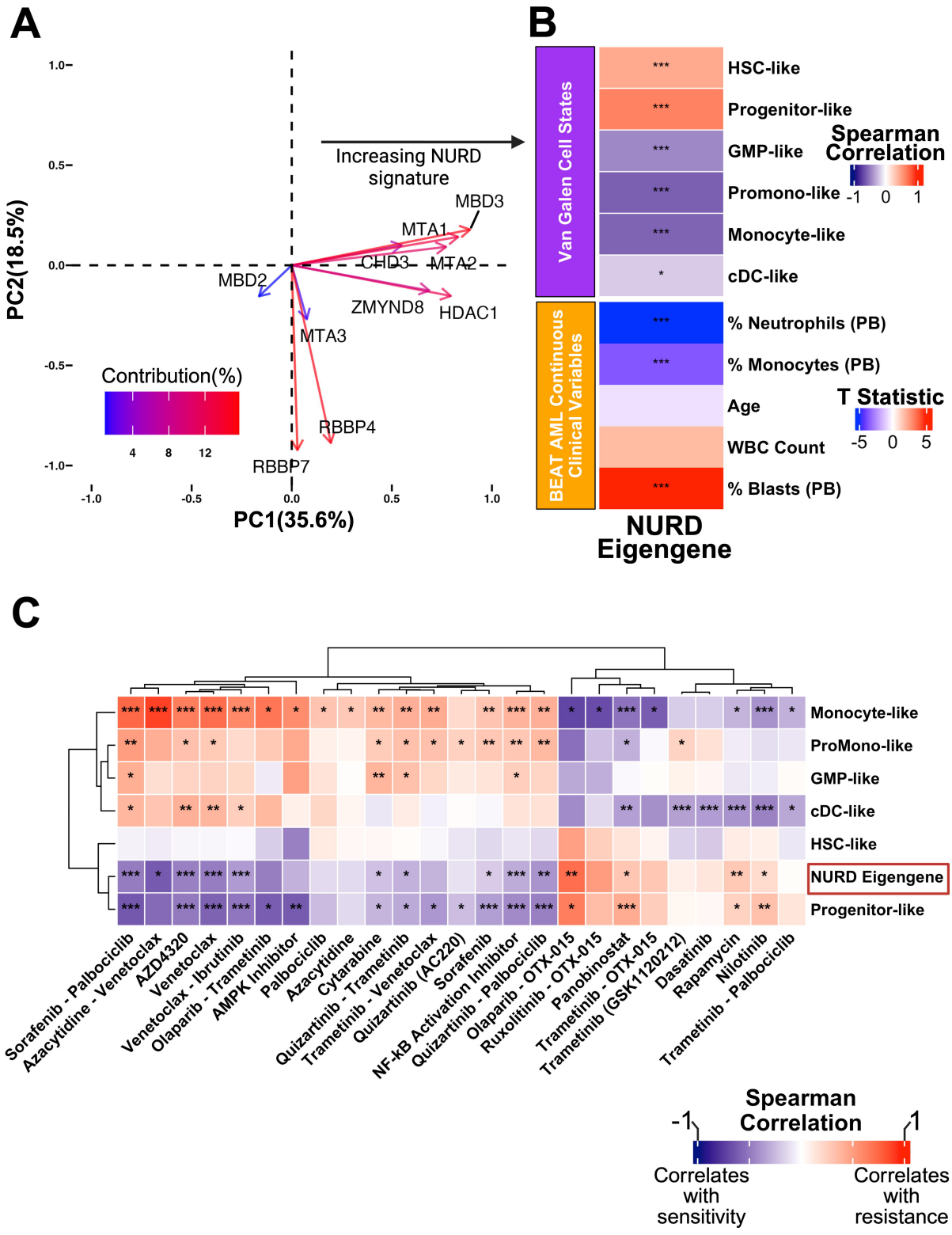
A
B
C
Increasing NURD signature
MBD3
MTA1
CHD3
MTA2
MBD2
ZMYND8
HDAC1
MTA3
RBBP4
RBBP7
Contribution(%)
4
8
12
PC1(35.6%)
PC2(18.5%)
Van Galen Cell States
HSC-like
Progenitor-like
GMP-like
Promono-like
Monocyte-like
cDC-like
BEAT AML Continuous Clinical Variables
% Neutrophils (PB)
% Monocytes (PB)
Age
WBC Count
% Blasts (PB)
NURD Eigengene
Spearman Correlation
T Statistic
Monocyte-like
ProMono-like
GMP-like
cDC-like
HSC-like
NURD Eigengene
Progenitor-like
Sorafenib - Palbociclib
Azacytidine - Venetoclax
AZD4320
Venetoclax
Venetoclax - Ibrutinib
Olaparib - Trametinib
AMPK Inhibitor
Palbociclib
Azacytidine
Cytarabine
Quizartinib - Trametinib
Trametinib - Venetoclax
Quizartinib (AC220)
Sorafenib
NF-kB Activation Inhibitor
Quizartinib - Palbociclib
Olaparib - OTX-015
Ruxolitinib - OTX-015
Panobinostat
Trametinib - OTX-015
Trametinib (GSK1120212)
Dasatinib
Rapamycin
Nilotinib
Trametinib - Palbociclib
Spearman Correlation
Correlates with sensitivity
Correlates with resistance

Supplemental Figures

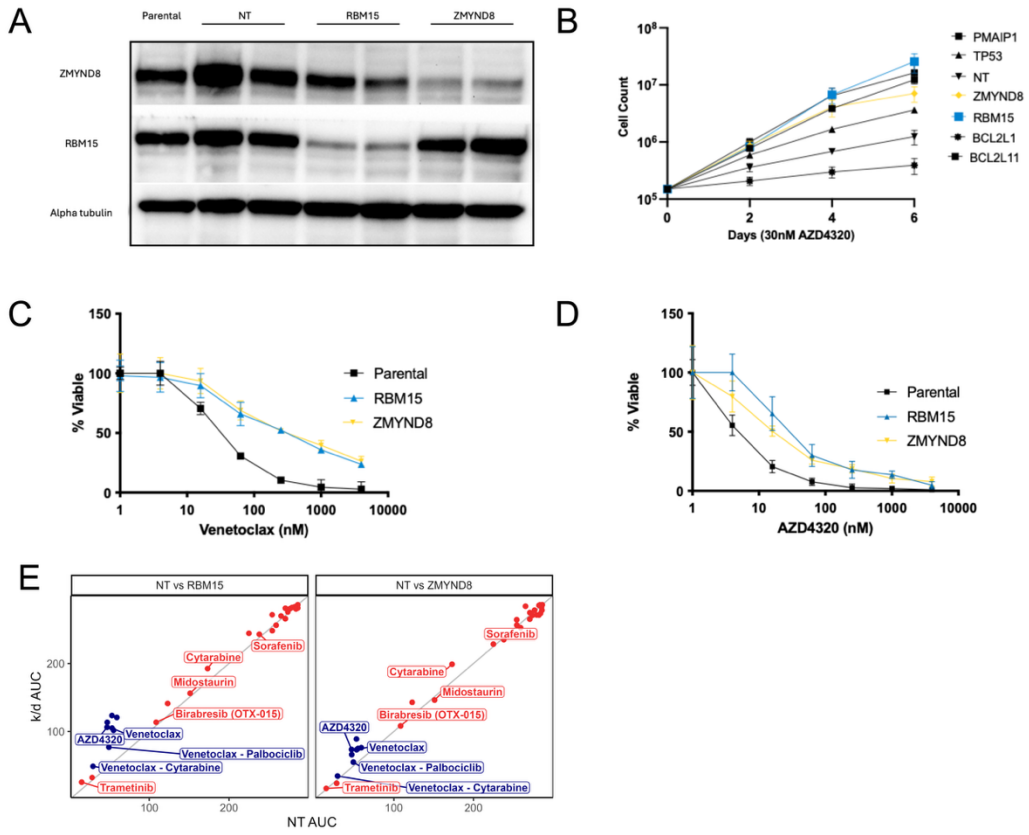

Supplemental Figure 1: Validation of CRISPR hits from AZD4320 CRISPR Screen. **(A)** Western blot analysis confirming CRISPR-Cas9-mediated knockout/down of RBM15 and ZMYND8. **(B)** Cell outgrowth assay performed on CRISPR-Cas9 knockout cell lines treated with 30 nM AZD4320, highlighting the drug resistance of *RBM15*-KO and *ZMYND8*-KO cells relative to non-targeting controls (NT). **(C)** Venetoclax sensitivity assay showing the dose-response curves for parental, *RBM15*-KO, and *ZMYND8*-KO cells following a 3-day variable concentration treatment. **(D)** AZD4320 sensitivity assay showing the dose-response curves for parental, *RBM15*-KO, and *ZMYND8*-KO cells following a 3-day variable concentration treatment. **(E)** Response of cell lines to a 3-day inhibitor panel, comparing RBM15-KO or ZMYND-KO OCI-AML2 cells (y-axis) to NT control cells (NT, x-axis). Response to venetoclax, AZD4320, or combinations including either are shown in blue.

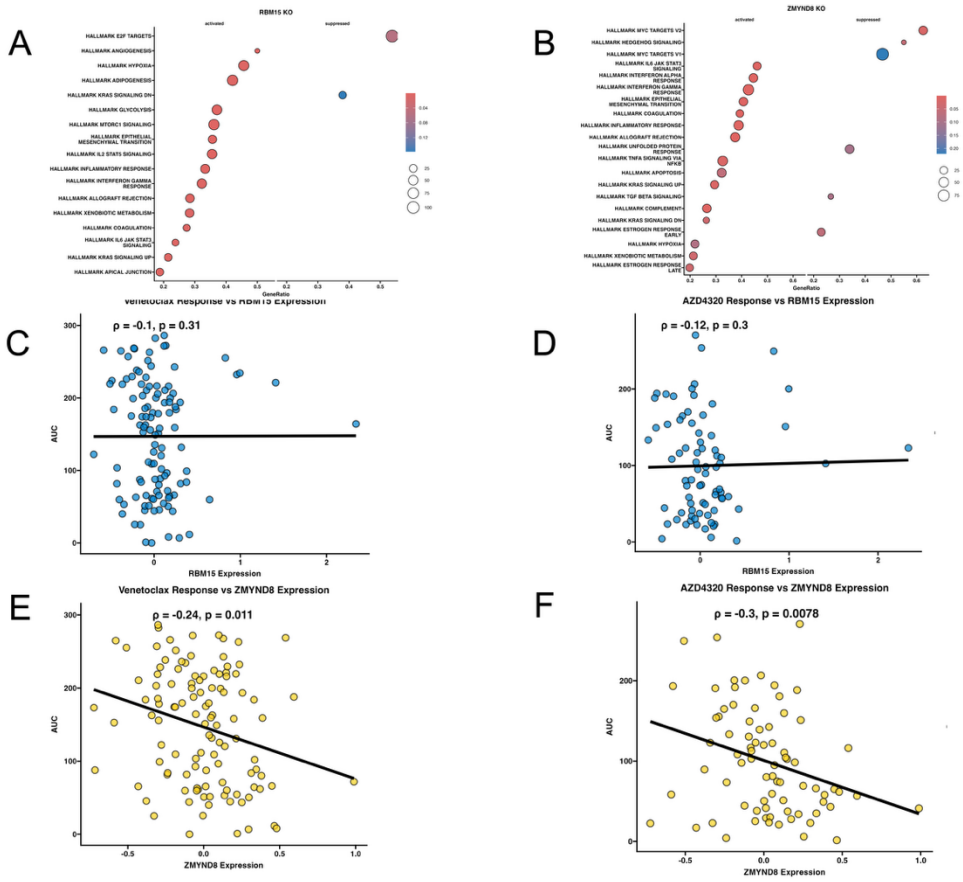

Supplemental Figure 2: Investigation of *RBM15* and *ZMYND8* in vivo and in vitro. **(A)** Gene Set Enrichment Analysis (GSEA) using hallmark pathways of differentially expressed genes between *ZMYND8*-KO and NT control cell lines, highlighting significantly enriched pathways. No significant pathway depletion was observed. **(B)** GSEA using hallmark pathways of differentially expressed genes between *RBM15*-KO and NT control cell lines, highlighting significantly enriched and depleted pathways. **(C-F)** Correlation between *RBM15* and *ZMYND8* protein expression in patient samples from Beat AML and the AUC values for AZD4320 and venetoclax, respectively.

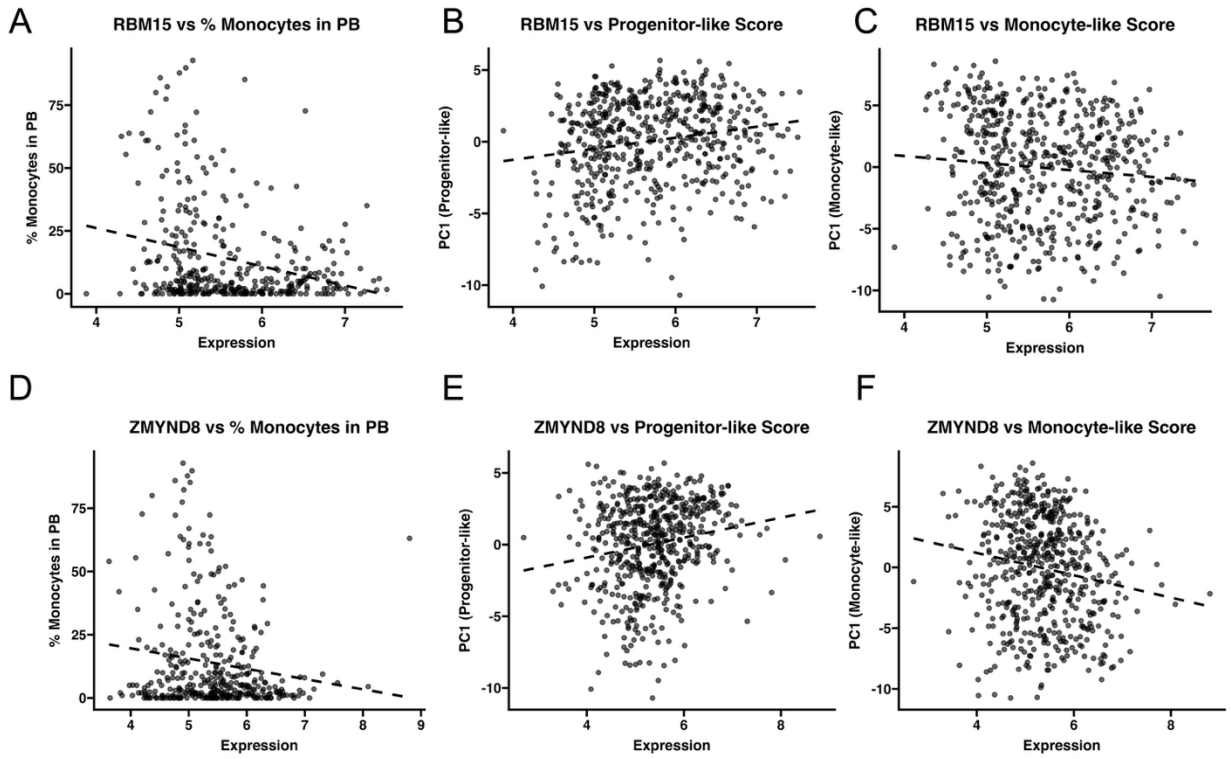

Supplemental Figure 3: RBM15 and ZMYND8 RNA expression correlates with differentiation-associated clinical and transcriptional markers.

(A–C) RBM15 expression plotted against (A) percent monocytes in peripheral blood (PB), (B) progenitor-like score, and (C) monocyte-like score.(D–F) ZMYND8 expression plotted against the same variables: (D) percent monocytes in PB, (E) progenitor-like score, and (F) monocyte-like score.

Percent monocytes in PB is a clinical measurement extracted from electronic medical records from patient from whom samples were obtained, while progenitor-like and monocyte-like scores are transcriptional estimates of differentiation derived from van Galen et al. cell state deconvolution. Linear regression lines are shown for visualization.

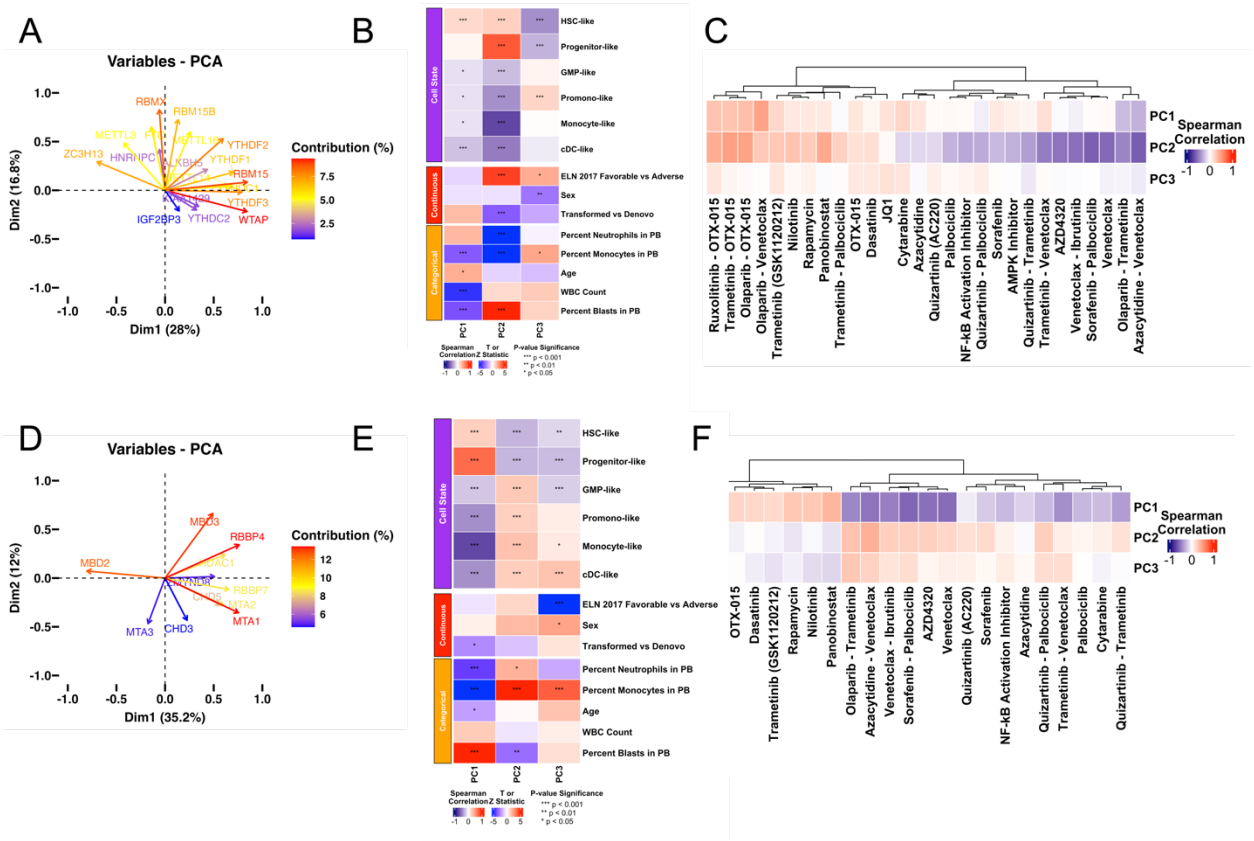

Supplemental Figure 4: m6a and NuRD RNA eigengenes correlate with cell differentiation state and AZD4320 AUC.

(A) Principal component analysis (PCA) biplot of m6A pathway gene RNA levels from the Beat AML dataset to generate an m6A eigengene-like signature. **(B)** Correlation of the m6A principal components with cell state scores and clinical differentiation markers, showing negative associations with more differentiated states in principal component 2 (PC2). **(C)** Drug response correlations for the m6A principal components, with PC2 being strongly correlated to resistance to AZD4320 and venetoclax. **(D)** PCA biplot of NuRD complex genes to create a NuRD eigengene-like signature. **(E)** Correlation of the NuRD principal components with cell states and differentiation markers, highlighting associations between PC1 and more differentiated cells. **(F)** Drug response correlations for the NuRD principal components, showing similar resistance patterns with PC1 to AZD4320 and venetoclax.

Supplemental Tables

m6a Family Gene List	NURD Family Gene List
METTL3	CHD3
METTL14	HDAC1
WTAP	CHD5
RBM15	MBD2
RBM15B	MBD3
METTL16	MTA1
KIAA1429	MTA2
ZC3H13	MTA3
IGF2BP1	RBBP4
IGF2BP3	RBBP7
YTHDC1	ZMYND8
YTHDC2	
YTHDF1	
YTHDF2	
YTHDF3	
HNRNPC	
HNRNPA2BP1	
FTO	
ALKBH5	
RBMX	
IGF2BP2	

Supplemental Table 1: Genes included in the m6A and NuRD pathway analyses. The m6A pathway gene list was curated through a literature review of known writers, readers, and erasers involved in m6A RNA methylation. The NuRD complex gene list was derived from the HUGO Gene Nomenclature Committee (HGNC) database definition for the NuRD complex gene family. These gene sets were used for principal component analyses and downstream pathway-level correlation analyses presented throughout the manuscript.

Target Gene	Sequence
RBM15_g1_F_1	GAGAGAGCAATTGGCCAATG
RBM15_g1_R_1	CATTGGCCAATTGCTCTCTC
RBM15_g2_F2	CCGATAGCGGCGGTGGGTCG
RBM15_g2_R2	CGACCCACCGCCGCTATCGG
ZMYND8_g1_F1	CTGTTTCAGCTTGGCTGAAG
ZMYND8_g1_R1	CTTCAGCCAAGCTGAAACAG
ZMYND8_g2_F2	CTTACTGAACAGTAACAATA
ZMYND8_g2_R2	TATTGTTACTGTTCAGTAAG

Supplemental Table 2: Primer sequences used for validation of RBM15 and ZMYND8 knockout cell lines.

Target	Antibody Product	Vendor	Species	Dilution
RBM15	25261	Cell Signaling	Rb	1:1000
ZMYND8	97845	Cell Signaling	Rb	1:1000
Vinculin	4650	Cell Signaling	Rb	1:1000

Supplemental Table 3: Antibodies used for Western blotting.

Supplemental Data Files (Excel)

Supplemental Data 1 (CRISPR Screen Results.xlsx):
Genome-wide CRISPR/Cas9 screen results comparing AZD4320-treated versus DMSO-treated OCI-AML2 cells. Contains sgRNA-level counts, $\log_2$ fold changes, p-values, and gene-level aggregation using the MAGeCK pipeline. Used for identifying genes mediating resistance to AZD4320.

Supplemental Data 2 (RNA Sequencing Results.xlsx):
Differential expression results from RNA sequencing of RBM15 and ZMYND8 knockout OCI-AML2 cells compared to non-targeting controls. Includes normalized counts, $\log_2$ fold changes, adjusted p-values (FDR), and gene annotations.

Supplemental Data 3 (BEAT AML AZD4320 Data.xlsx):
Drug response data from the Beat AML dataset, including AZD4320 area under the curve (AUC) values (derived from a probit regression as in *Bottomly, 2022*).Used in correlation analyses with gene expression and cell state features.

Supplemental Methods

Cell Lines and Culture Conditions

Human AML cell line OCI-AML2 was obtained from the ATCC and authenticated using short tandem repeat (STR) profiling at the OHSU DNA Services Core Facility. Cells were maintained in RPMI-1640 medium (Gibco, Thermo Fisher Scientific, Waltham, MA, USA, #11875093) supplemented with 20% fetal bovine serum (FBS; Gibco, #10437028), 2mM L-glutamine(Gibco, #25030081), 100 U/mL penicillin-streptomycin(Gibco, #15140122), and 0.25 µg/mL amphotericin B (Gibco, #15290018). Cultures were incubated at 37 °C in a humidified atmosphere with 5% CO_2 and passaged every 2–3 days. Mycoplasma contamination was routinely checked.

Genome-Wide CRISPR/Cas9 Screening

Loss-of-function screens were performed using the Y. Kosuke human genome-wide sgRNA library (Addgene, Watertown, MA, USA, #67989). OCI-AML2 cells expressing Cas9 were generated by transduction with lentivirus carrying the Cas9 construct, followed by selection with blasticidin [10 μg/mL] (InvivoGen, San Diego, CA, USA, #ant-bl-1) for 5-7 days to ensure stable integration. Approximately 1×10^8 transduced cells were used to maintain a library coverage of >500 cells per sgRNA.

Cells were transduced with the Y. Kosuke library lentivirus at a multiplicity of infection (MOI) of 0.3 and selected with puromycin (2 μg/mL) for 7 days. Following selection, cells were divided into treatment and control groups. The treatment group was exposed to 30 nM AZD4320 for 14 days, while control cells were treated with an equivalent volume of DMSO (final concentration: 0.1%). Genomic DNA was harvested at days 0, 7, and 14 for downstream analysis.

Genomic DNA was extracted using phenol-chloroform, and sgRNA libraries were amplified using a one-step PCR method to attach Illumina barcodes and primers. Pooled PCR products were sequenced on an Illumina platform. Enriched or depleted sgRNAs were identified by comparing AZD4320-treated and control (DMSO) samples using MAGeCK analysis pipeline described in our previous study.[7] The robust rank aggregation method was applied to compute gene-level p-values, which were adjusted for multiple testing using the Benjamini-Hochberg procedure. Genes with an FDR <0.05 were considered significant.

CRISPR screen hits were tiered using a method previously described by Nechiporuk et al. (2019). Briefly, sgRNA-level hits were ranked based on three key criteria: effect size ($\log_2$-fold change), concordance among guides targeting the same gene, and the number of supporting sgRNAs per gene. A minimum read count of 100 and an FDR < 0.05 were required for inclusion. Tier 1 hits had $\log_2$-fold change > 2, >75% of sgRNAs per gene scoring, and >75% concordance among those sgRNAs. Tier 2 hits required $\log_2$-fold change > 2 and 100% guide concordance. Tier 3 hits had $\log_2$-fold change > 1 and 100% concordance. An additional category of high-confidence

single-guide hits ("singletons") was defined by a $\log_2$-fold change > 2, FDR < 0.05, and only one targeting guide with >100 reads in the control.

Generation and Validation of Knockout Cell Lines

Lentiviral particles were produced in HEK293T cells by co-transfecting the cells with psPAX2 packaging plasmid (Addgene, #12260), and pMD2.G envelope plasmid (Addgene, #12259) using Lipofectamine 2000 (Invitrogen, #11668019). Viral supernatants were collected at 48- and 72-hours post-transfection, filtered through a 0.45 µm filter, and concentrated by ultracentrifugation at 25,000 rpm for 2 hours at 4 °C.

OCI-AML2 cells were transduced with single guides at an MOI of approximately 0.3 to ensure single integrations per cell. Transduction was performed in the presence of 8 µg/mL Polybrene (Sigma-Aldrich, #TR-1003-G) by spinoculation at 1,000 × g for 2 hours at 32 °C. Transduced cells were selected with puromycin (2 µg/mL) for 7 days to establish stable integration before drug treatment. Knockout efficiency was validated by Western blotting.

Protein lysates were prepared using RIPA buffer supplemented with protease (Roche, #11836170001) and phosphatase inhibitors(ThermoFisher Scientific, #AAJ61022AA). Protein concentrations were determined using the Pierce BCA protein assay (ThermoFisher Scientific, #23227). Samples (30 µg per lane) were separated by SDS-PAGE on 4-15% polyacrylamide gels (Bio-Rad, Hercules, CA, USA, #4561084) and transferred to PVDF membranes (MilliporeSigma, #IPVH00010). Membranes were blocked with 5% bovine serum albumin (BSA) in Tris-buffered saline with 0.1% Tween-20 (TBST) for 1 hour at room temperature and incubated overnight at 4 °C with primary antibodies. After washing with TBST, membranes were incubated with HRP-conjugated secondary antibodies for 1 hour at room temperature. Bands were visualized using Clarity chemiluminescence (ECL) (Bio-rad, #1705061) substrate and imaged using a ChemiDoc Imaging System (Bio-Rad, #1708280). Antibody details are provided in the supplemental table 3.

Cell Proliferation and Viability Assays

Wild-type (WT), non-targeting control (NT), RBM15 knockout (RBM15 KO), and ZMYND8 knockout (ZMYND8 KO) OCI-AML2 cells were seeded at an initial density of 2×10^5 cells/mL in T25 flasks containing 5 mL of complete medium with 30 nM AZD4320 or DMSO. Cells were cultured for 6 days, and viable cell counts were performed every 2 days.

For dose-response assays, cells were seeded in 96-well plates at 1×10^4 cells per well in triplicate and treated with serial dilutions of venetoclax or AZD4320 ranging from 0.01 nM to 10 μm. After 72 hours of incubation at 37 °C, cell viability was determined by addition of MTS reagent (CellTiter96 AQueous One; Promega Madison, WI, USA) and measurement of absorbance at 490nm. Luminescence was measured using a SpectraMax iD3 microplate reader. Half-maximal inhibitory concentration (IC_{50}) values were calculated using nonlinear regression analysis in GraphPad Prism 10 software.

RNA Sequencing and Preprocessing

Total RNA was extracted from OCI-AML2 wild-type, non-targeting control (NT), RBM15 knockout, and ZMYND8 knockout cells using the RNeasy Mini Kit (Qiagen) with on-column DNase digestion to eliminate genomic DNA. RNA quality and quantity were assessed using a NanoDrop spectrophotometer. RNA sequencing libraries were prepared using stranded poly(A)+ selection and sequenced on an Illumina NovaSeq 6000 platform, generating 150 base pair paired-end reads at a target depth of approximately 50 million read pairs per sample.

Paired-end BAM files were aligned to the GRCh38 human reference genome and quantified at the gene level using the featureCounts function with Ensembl gene annotations. Only genes with counts of at least 10 in at least 90% of samples were

retained. Genes with invalid Ensembl IDs or all-zero counts were removed. Ensembl gene identifiers were mapped to HGNC symbols using the org.Hs.eg.db reference database.

Sample condition metadata were extracted from file names and used to classify samples into one of four groups: NT, RBM15, ZMYND8, or parental. Any missing values in the count matrix were set to zero. The resulting filtered count matrix and metadata were used for downstream normalization and differential expression analysis.

Differential Expression and Downstream Analysis

Differential expression analysis was conducted using the DESeq2 framework with negative binomial modeling and dispersion estimation. Surrogate variable analysis (SVA) was performed on the raw count matrix to estimate unmeasured sources of variation. The resulting surrogate variables were incorporated into the design formula for differential testing. Condition labels were set with NT as the reference group.

Differential expression testing was performed for all pairwise comparisons among experimental groups. Genes with an adjusted p-value (Benjamini-Hochberg correction) less than 0.05 were considered statistically significant. No fold-change threshold was applied. Differential expression results, including $\log_2$ fold change, nominal p-values, and adjusted p-values, were exported for downstream analyses and visualization.

Enrichment, Correlation, and Heatmap Analyses

Gene set enrichment analysis was performed using preranked gene lists based on DESeq2 test statistics. Enrichment was assessed against Hallmark gene sets from the Molecular Signatures Database (MSigDB). Enrichment significance was reported using normalized enrichment scores (NES), nominal p-values, and false discovery rate–adjusted q-values.

Cell type enrichment analysis was conducted using curated lineage-specific marker genes from PanglaoDB. Genes significantly upregulated in knockout conditions were tested for enrichment. Multiple hypothesis correction was applied using the Benjamini-Hochberg method.

For correlation analyses, eigengene-derived scores representing hematopoietic cell states were obtained from previously published methods.[36] These scores were correlated with RBM15 and ZMYND8 expression using Spearman correlation. Statistical significance was calculated using two-sided tests. Heatmaps were generated using normalized expression values or $\log_2$ fold changes. Genes and samples were clustered using hierarchical clustering with Euclidean distance and complete linkage.

m⁶A and NuRD Complex Analyses (Protein and RNA)

To evaluate the relationship between m⁶A and NuRD complex gene expression and clinical phenotypes, curated gene sets were compiled for each complex. m⁶A family members were selected based on published literature, and NuRD complex components were obtained from the HUGO Gene Nomenclature Committee.

Protein-level expression data were obtained from the PNNL proteomics dataset. RNA-level expression was sourced from the BEAT AML RNA-seq dataset. The resulting principal component scores were merged with BEAT AML clinical annotations, including drug response data (AUC values), cell state scores (vg type and PC1), and other relevant variables. Associations between PCA-derived scores and clinical features were explored using linear regression and correlation, with visualization approaches as described in the relevant figure legends.